SCIENTIFIC REPORTS

OPEN

SUBJECT AREAS:
ORGANIC LEDS
MATERIALS FOR DEVICES
LEDS AND LIGHT SOURCES

Received
23 October 2014

Accepted
19 January 2015

Published
12 February 2015

Correspondence and requests for materials should be addressed to C.A. (adachi@cstf.kyushu-u.ac.jp)

* These authors contributed equally to this work.

Dual enhancement of electroluminescence efficiency and operational stability by rapid upconversion of triplet excitons in OLEDs

Taro Furukawa[1]*, Hajime Nakanotani[1,2]*, Munetomo Inoue[1] & Chihaya Adachi[1,2,3]

[1]Center for Organic Photonics and Electronics Research (OPERA), Kyushu University, 744 Motooka, Nishi, Fukuoka 819-0395, Japan, [2]JST, ERATO, Adachi Molecular Exciton Engineering Project, c/o Center for Organic Photonics and Electronics Research (OPERA), Kyushu University, 744 Motooka, Nishi, Fukuoka 819-0395, Japan, [3]International Institute for Carbon Neutral Energy Research (WPI-I2CNER), Kyushu University, 744 Motooka, Nishi, Fukuoka 819-0395, Japan.

Recently, triplet harvesting *via* a thermally activated delayed fluorescence (TADF) process has been established as a realistic route for obtaining ultimate internal electroluminescence (EL) quantum efficiency in organic light-emitting diodes (OLEDs). However, the possibility that the rather long transient lifetime of the triplet excited states would reduce operational stability due to an increased chance for unwarranted chemical reactions has been a concern. Herein, we demonstrate dual enhancement of EL efficiency and operational stability in OLEDs by employing a TADF molecule as an assistant dopant and a fluorescent molecule as an end emitter. The proper combination of assistant dopant and emitter molecules realized a "one-way" rapid Förster energy transfer of singlet excitons from TADF molecules to fluorescent emitters, reducing the number of cycles of intersystem crossing (ISC) and reverse ISC in the TADF molecules and resulting in a significant enhancement of operational stability compared to OLEDs with a TADF molecule as the end emitter. In addition, we found that the presence of this rapid energy transfer significantly suppresses singlet-triplet annihilation. Using this finely-tuned rapid triplet-exciton upconversion scheme, OLED performance and lifetime was greatly improved.

Since organic light-emitting diodes (OLEDs) possess extremely attractive properties such as highly efficient electroluminescence (EL), flexibility, lightweight, and the possibility of solution processing and low-cost manufacture, they are fascinating for advanced full-color flat-panel displays and lighting applications. In particular, improvement of the internal EL quantum efficiency (η_{int}) is a fundamental issue since one singlet exciton is generated for every three triplet excitons in the event of carrier recombination[1]. Thus, η_{int} is limited to as low as 25% when using highly emissive fluorescent molecules even if their photoluminescence (PL) quantum yields (Φ_{PL}) are nearly 100%.

To improve η_{int} by harvesting triplet excitons, several unique routes have been proposed. The most well established route is the utilization of room-temperature phosphorescence emitters, such as iridium (Ir) or platinum (Pt) complexes, as an emissive dopant. Since the presence of heavy metals such as Ir and Pt induces mixing between the singlet state (S_1) and the triplet state (T_1) due to spin-orbital coupling, phosphorescence-based OLEDs (**PHOS-OLEDs**) can achieve an ultimate η_{int} of nearly 100% even at room temperature[2–6]. Another potential route to generate singlet excitons that has been reported is triplet–triplet annihilation (TTA)[7–10]. However, the maximum fraction of triplets that can be converted to singlets by the TTA process is 50%, resulting in an upper limit for the radiative exciton production efficiency (η_r) of less than 62.5% (= 25% + 75% × 0.5)[11].

In our recent works, on the other hand, we demonstrated an alternative route to harvest triplet excitons by utilizing a thermally activated delayed fluorescence (TADF) process[12–16], *i.e.*, "**TADF-OLEDs**". In the TADF process, generated triplet excitons can be thermally upconverted into an S_1 state through reverse intersystem crossing (RISC) because of a small energy gap (ΔE_{ST}) between the S_1 and T_1 states, and light emission can be extracted as a delayed fluorescence from the S_1 state. Based on a sophisticated molecular design, we have reported a series of highly efficient OLEDs with TADF emitters demonstrating η_{int} of nearly 100%[14].

Furthermore, we recently designed a novel device architecture with the proper combination of TADF molecule as a singlet exciton generator and fluorescent molecule as an end emitter, *i.e.*, TADF-assisted fluorescence, hereafter abbreviated as "**TAF-OLED**", that enables η_{int} of nearly 100% from conventional fluorescent emitters and has great potential for improving operational stability[17]. However, the operational stability is still unsatisfactory compared to state-of-the-art fluorescence-based OLEDs (**FLU-OLEDs**). Since very few reports on the operational stability of OLEDs incorporating TADF molecules are available[16], guidelines for obtaining high operational stability in these devices are desired.

In the early stage of OLEDs starting in 1950's, emitter layers were composed of fluorescent molecules that can harvest only singlet excitons. Advances in molecules exhibiting room temperature phosphorescence since 1998 led to achievement of nearly 100% radiative decay from triplet excited states. From 2012, newly invented TADF molecules allow for 100% upconversion from triplet into singlet states, leading to nearly 100% of excited states contributing to radiative decay from singlet states. Now, more than 50 years after the first observation of EL from fluorescent molecules, **TAF-OLED**s have realized emission from conventional fluorescence molecules utilizing nearly 100% of the created excitons.

In this report, we establish basic guidelines for enhancing the stability of **TAF-OLEDs**: the TADF assistant dopant should have a high RISC rate constant (k_{RISC}) and Förster resonance energy transfer (FRET) from the TADF molecules to the fluorescent emitters should be a rapid, one-way process. Meeting these criteria reduces the number of cycles of intersystem crossing (ISC) and RISC in the TADF molecule, enabling high operational stability and high η_{EQE} at high luminances through reduced triplet populations and the suppression of a bimolecular recombination processes.

Results

Energy transfer process. Figure 1(a) shows schematic illustrations of the energy transfer systems for **TADF-OLED**s (left) and **TAF-OLED**s (right), highlighting that light is emitted from TADF molecules and fluorescent molecules, respectively, in each system. In this work, we used (2s,4r,6s)-2,4,5,6-tetrakis(3,6-dimethyl-9H-carbazol-9-yl) isophthalonitrile (4CzIPN-Me)[18] as an assistant dopant and 2,8-di[t-butyl]-5,11-di[4-(t-butyl)phenyl]-6,12-diphenylnaphthacene (TBRb) as a fluorescent emitter. Since this combination showed a large spectral overlap between the absorption spectrum of TBRb and the PL spectrum of 4CzIPN-Me (Fig. 1(b)), efficient FRET of singlet excitons from the exciton donor (4CzIPN-Me) to the exciton acceptor (TBRb) is possible even at a TBRb concentration of 0.65 mol% due to a rather large Förster transfer radius (R_0)[19] of ~7.4 nm. In this study, to prevent direct energy transfer of the triplet excitons from 4CzIPN-Me to TBRb *via* Dexter energy transfer, 4CzIPN-Me and TBRb were doped into a 3,3-di(9H-carbazol-9-yl)biphenyl (mCBP) host matrix at finely-tuned concentrations of 6.3 mol% and 0.65 mol%, respectively, minimizing the number of adjacent 4CzIPN-Me and TBRb molecules (see Supplementary note). As host, mCBP was chosen for its wide energy gap and high triplet energy of 2.9 eV, which confines triplet excitons to the dopant molecules[20].

To confirm that energy transfer occurs from the 4CzIPN-Me molecules to the TBRb emitters, transient PL decay curves were measured for 0.65mol%-TBRb: 6.3mol%-4CzIPN-Me: mCBP and 6.3mol%-4CzIPN-Me: mCBP co-deposited films (Supplementary Figure 2). Identical emission spectra for the delayed and prompt components, which originate from TBRb, were observed in the 0.65mol%-TBRb: 6.3mol%-4CzIPN-Me: mCBP film. In addition, the delayed emission intensity is reduced in the film with 0.65mol% TBRb compared to that of the film without TBRb, indicating that singlet excitons of 4CzIPN-Me are promptly transferred to the S_1 state of TBRb *via* FRET as opposed to *via* the reabsorption of 4CzIPN-Me emission by TBRb, in which case the delayed emission intensities would be nearly the same.

Furthermore, the energy transfer efficiency from an energy donor to an energy acceptor can be estimated by

$$E = 1 - \frac{F_{DA}}{F_D}. \quad (1)$$

Here, E is the energy transfer efficiency and F_{DA} and F_D are the spectral Φ_{PL} at the same wavelength for donor emission in a matrix with and without acceptor molecules, respectively. As shown in Supplementary Figure 3, the spectral Φ_{PL} of donor molecules at a wavelength of 500 nm was significantly reduced by the presence of acceptor molecules, indicating efficient energy transfer with an E of ~0.8 calculated from F_{DA} of $\sim 7.9 \times 10^{-4}$ nm^{-1} and F_D of $\sim 3.3 \times 10^{-3}$ nm^{-1}.

OLED characteristics. The energy diagram of the fabricated OLEDs is shown in Fig. 1(c) (device architecture details can be found in the Methods section). In addition to the **TAF-** and **TADF-OLED**s, **FLU-OLED**s with only TBRb as emitter, and no 4CzIPN-Me, doped into an mCBP host were also made for reference. The performance of the three devices, **TAF-OLED** (red), **TADF-OLED** (blue), and **FLU-OLED** (black), are summarized in Table 1 and Fig. 2. While the **FLU-OLED** showed a maximum external EL quantum efficiency (η_{EQE}) of 4 ± 1% at 7 cd m^{-2}, the **TADF-OLED** with 4CzIPN-Me as an emitter showed the highest η_{EQE} of 21.0 ± 1% at 185 cd m^{-2}, indicating that η_r approaches 94 ~ 100% using a Φ_{PL} of 74 ± 3% measured for a 6.3mol%-4CzIPN-Me: mCBP co-deposited film and assuming an ideal charge balance factor of unity and a light out-coupling efficiency of 20~30%[21,22].

On the other hand, in the **TAF-OLED** with 4CzIPN-Me as an assistant dopant, the emission from 4CzIPN-Me was significantly reduced, and the device exhibited light emission mainly originating from TBRb (Fig. 2(b)) with a high η_{EQE} of 19.1 ± 1% at 20 cd m^{-2}, indicating high η_r of 78.6 ~ 100% using a Φ_{PL} of 81 ± 3% from a 0.65mol%-TBRb: 6.3mol%-4CzIPN-Me: mCBP co-deposited film and clearly confirming that the **TAF-OLED** overcame the upper limit of η_r = 25% assumed for fluorescent emitters. In addition, although η_{EQE} rapidly drops to 62.5% of its maximum value at 800 cd m^{-2} in the **FLU-OLED**, the **TAF-OLED** maintained high η_{EQE} of 17.5 ± 1%, 16.7 ± 1%, 14.1 ± 1%, and 12.5 ± 1% even at high practical luminances of 500, 1,000, 5,000, and 10,000 cd/m^2, corresponding to 92%, 87%, 74%, and 65% of the maximum η_{EQE}, respectively. These high values indicate that the exciton annihilation process is significantly suppressed in the **TAF-OLED** compared to the **FLU-OLED** (Fig. 2(a)).

The η_{EQE} of 19.1 ± 1% is the highest efficiency in OLEDs with a classical fluorescent molecule as the end emitter. The slightly lower η_{EQE} than for the **TADF-OLED** is probably due to holes injected from the TAPC hole transport layer into the emitter layer (EML) being directly trapped by TBRb molecules because of the shallower highest occupied molecular orbital (HOMO) level of TBRb (−5.4 eV) compared to that of 4CzIPN-Me (−5.9 eV) (see Fig. 1(c)). In fact, a slight increase of the driving voltage for the **TAF-OLED** compared to that of the **TADF-OLED** was observed (Fig. 2(b) inset), supporting the proposal of partial direct trapping on the TBRb molecules.

Device operational stability. Although the **TADF-** and **TAF-OLED**s had comparable η_{EQE}, the operational lifetimes of these OLEDs were pronouncedly different. Figure 2(c) compares the EL intensity of the **TADF-** and **TAF-OLED**s as a function of time operated at a constant current starting at an initial luminance of L_0 = 1,000 cd m^{-2}. We found that the operational lifetime *LT50*, which is defined as the time when the luminance drops to 0.5 of the initial luminance, of the **TAF-OLED** was 3,775 hours and is over 2.5 times

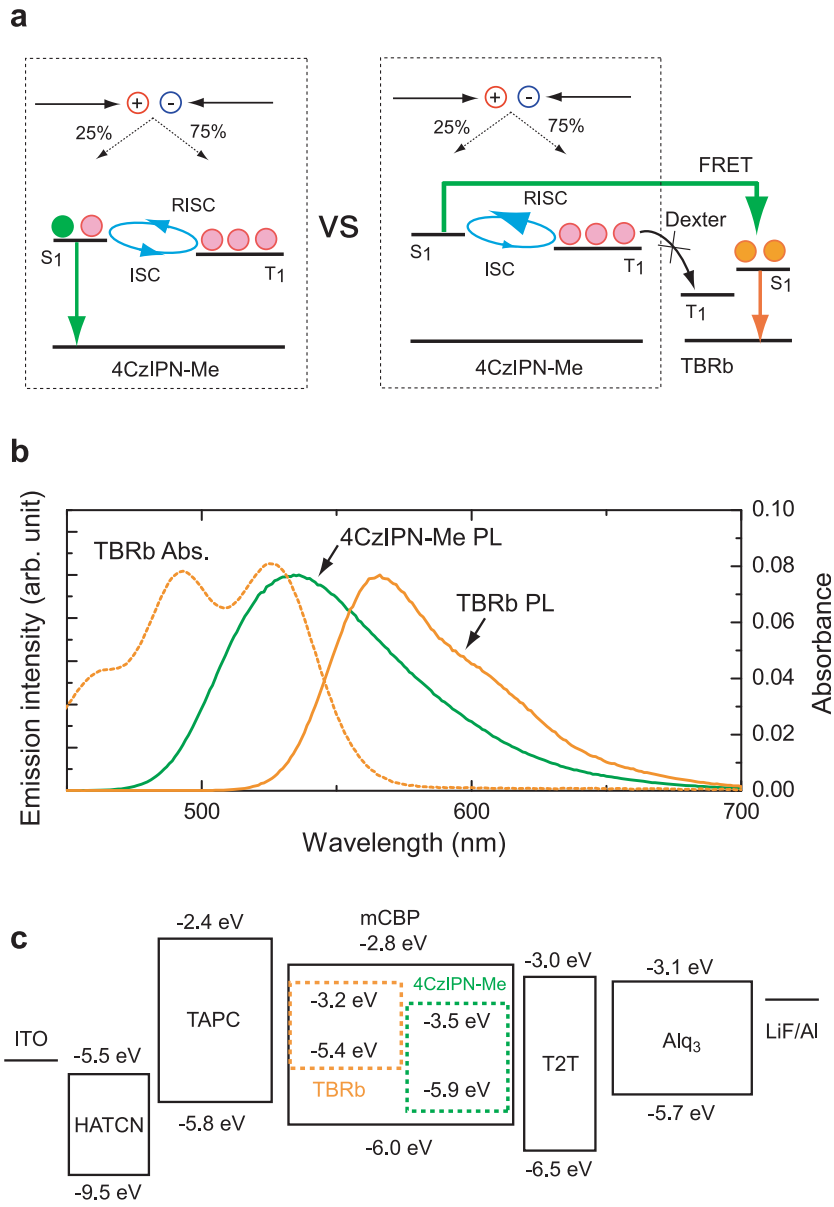

Figure 1 | Energy diagram. (a) Schematic illustration of the conceived energy transfer mechanism for the 4CzIPN-Me (assistant dopant):TBRb (fluorescent emitter) system under electrical excitation (right). The left figure shows a conventional energy diagram for 4CzIPN-Me as emitter. (b) PL spectra of a 11mol%-4CzIPN-Me:mCBP co-deposited film and TBRb solution (CH_2Cl_2, 10^{-5} mol L^{-1}). The dashed line indicates the absorption spectrum of the TBRb solution (CH_2Cl_2, 10^{-5} mol L^{-1}). The Förster radius was obtained from the overlap of the PL spectrum of the exciton donor and the absorption spectrum of the exciton acceptor based on the assumptions of random molecular orientation and a refractive index of 1.8 for the mCBP medium. (c) Energy diagram of the OLEDs used in this work. HOMO levels were measured by photoelectron spectroscopy (Riken Keiki, AC-3). Energy gaps were estimated from the absorption edges of neat films.

longer than that of the **TADF-OLED** (*LT50* = 1,470 hours) while the voltage-rise curves are almost the same for both OLEDs as shown in the inset of Fig. 2(c).

Although the electrochemical stability of the final emitter, *i.e.*, TBRb, will also affect the operational stability of the **TAF-OLED**, the enhanced stability while maintaining a high η_{EQE} for the **TAF-**

Table 1 | Device performance of the tested OLEDs

EML	Turn-on voltage [V]	Max. η_{EQE} [%]	Max. CE [cd A^{-1}]	CIE [a]	Performance at 1,000 cd m^{-2}			LT50 [hour]
					Voltage [V]	η_{EQE} [%]	CE [cd A^{-1}]	
TBRb	6.0	4.0	13	(0.43, 0.51)	10[b]	2.5[b]	7.9[b]	5
4CzIPN-Me	3.8	21.0	73	(0.37, 0.58)	6.6	19.7	68	1,472
TBRb: 4CzIPN-Me	4.0	19.1	62	(0.43, 0.54)	7.5	16.7	56	3,775

[a]The CIE were obtained at 500 cd m^{-2}.
[b]These values were obtained at 800 cd m^{-2}.

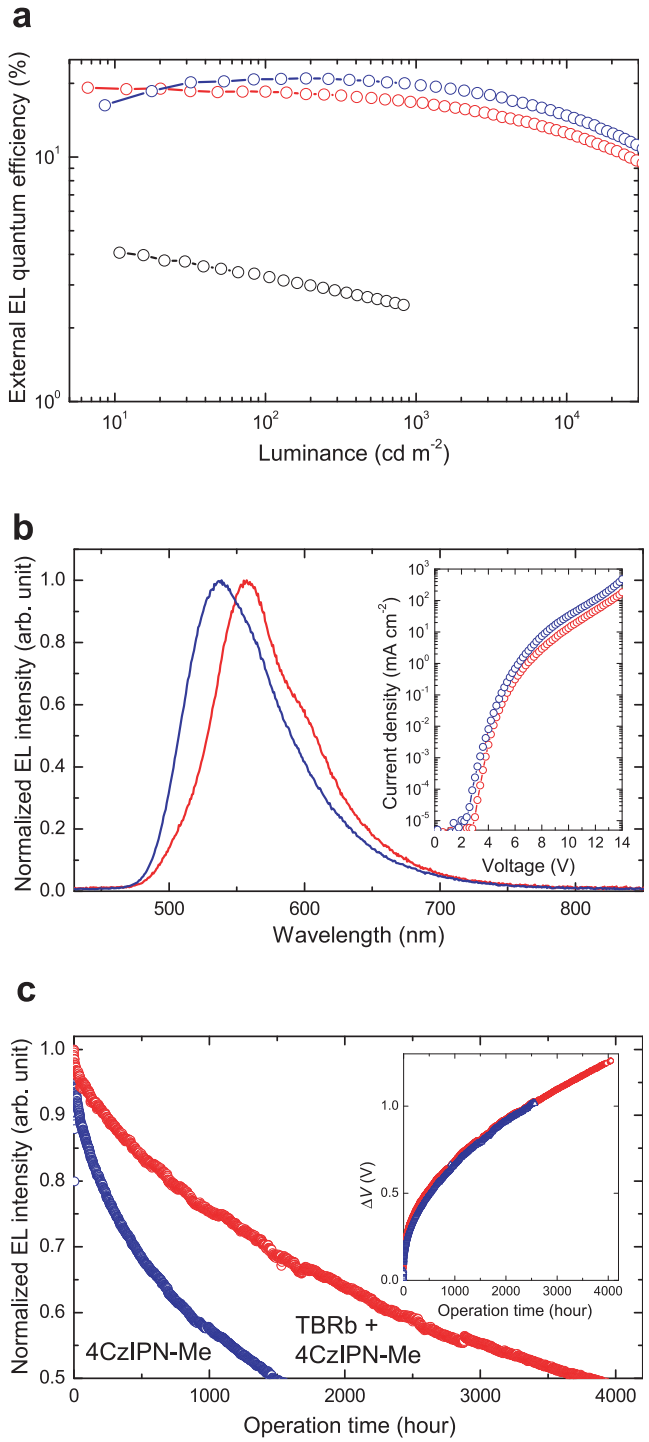

Figure 2 | OLED performance. (a) External EL quantum efficiency as a function of luminance for the tested OLEDs. The black, blue and red circles showed the device performance for the OLEDs with TBRb only (**FLU-OLED**), 4CzIPN-Me only (**TADF-OLED**) and TBRb:4CzIPN-Me (**TAF-OLED**), respectively. (b) Normalized EL spectra of the OLEDs with 4CzIPN-Me as emitter (blue, **TADF-OLED**) and 4CzIPN-Me as assistant dopant (red, **TAF-OLED**) at 500 cd m^{-2}. Inset: Current density – voltage characteristics of these devices (coloured accordingly). (c) Operational stability of the tested OLEDs. Initial luminance is set to 1,000 cd m^{-2} for all devices. The injected current density is constant at 1.9 mA cm^{-2} and 2.1 mA cm^{-2} for the OLEDs with 4CzIPN-Me as emitter (**TADF-OLED**) and as assistant dopant (**TAF-OLED**), respectively. Inset: Voltage rise curves for the tested devices (coloured accordingly).

OLED compared to the **TADF-OLED** is mainly attributed to rapid FRET from 4CzIPN-Me to TBRb since carrier recombination still mainly occurs on the TADF molecules in the **TAF-OLED**. We note that the operational stability (*LT50* = 3,775 hours) of the **TAF-OLED** with 4CzIPN-Me as an assistant dopant was also significantly longer than that of an OLED with the phenoxazine derivative 2-phenoxazine-4,6-diphenyl-1,3,5-triazine (PXZ-TRZ)[13] as assistant dopant (950 hours for an initial luminance of 1,000 cd m^{-2} and 194 hours operated at a constant current density of 10 mA cm^{-2})[17], suggesting that the electrochemical stability of the assistant dopants also affects the operational stability. Since the long lifetime nature of triplet excitons has been suspected as a cause of device degradation[23], an assistant dopant with a short triplet lifetime may decrease the chance for chemical degradation.

Another aspect that can affect device stability is the thin-film morphology. Although partial crystallization was observed in a 0.65mol%-TBRb:mCBP film after storage in a nitrogen atmosphere for a few days, no changes of film morphology were observed in 6.3mol%-4CzIPN-Me:mCBP and 0.65mol%-TBRb:6.3mol%-4CzIPN-Me: mCBP films, suggesting that crystallization is well suppressed for the films doped with 6.3 mol% 4CzIPN-Me (see Supplementary note).

Exciton dynamics in TAF-OLEDs. Focusing on the electrically-driven degradation of the devices, the operation mechanism for enhancing the device stability in the **TAF-OLED** was studied in more detail. An important factor that may enable an enhancement of operational stability is the decrease of ISC/RISC cycles, and thereby the triplet population, due to the presence of rapid energy transfer *via* a Förster process. In the case of the **TADF-OLED**, triplet excitons that are electrically generated on 4CzIPN-Me are promptly converted to the S_1 state through RISC with a rate constant of $k_{RISC} = 7.7 \times 10^5$ s^{-1}, which is realized due to the small $\Delta E_{ST} = 0.05$ eV (see Supplementary note). The singlet excitons then have two possible decay pathways: (1) radiative decay from the S_1 state to the ground state (S_0) with a radiative decay rate of $k_r^S = 2.5 \times 10^7$ s^{-1}, or (2) ISC back to the T_1 state of 4CzIPN-Me with a rate constant of $k_{ISC} = 4.1 \times 10^7$ s^{-1}. The triplet excitons resulting from ISC can subsequently upconvert again, and these competitive decay and upconversion processes will be repeated until all of the excitons finally decay as light emission or heat dissipation.

On the other hand, when fluorescent molecules, *i.e.*, TBRb, are added to the mixed matrix, *i.e.*, **TAF-OLEDs**, an additional decay path from the singlet excited state, *i.e.*, FRET from the S_1 state of 4CzIPN-Me to the S_1 state of TBRb, is now available. In this case, the singlet and triplet density dynamics of 4CzIPN-Me under optical excitation can be described by

$$\frac{dN_S}{dt} = -k_{ET}N_S - k_r^S N_S - k_{ISC}N_S + k_{RISC}N_T + P, \quad (2)$$

$$\frac{dN_T}{dt} = -k_{nr}^T N_T - k_{RISC}N_T + k_{ISC}N_S, \quad (3)$$

where k_{ET} is the rate constant of energy transfer from a TADF molecule to a fluorescent emitter, N_S and N_T denote the singlet and triplet densities, respectively, and P is the density of singlet excitons generated by optical excitation. Since the rate constant of FRET, $k_{ET} = \left(1/\tau_D\right)\left(R_0^6/R^6\right)$, where τ_D is radiative decay time of donor molecular and R is the average distance between donor and acceptor molecules (~4.6 nm for this TAF film), is nearly two orders of magnitude faster than those of the ISC and RISC processes, *i.e.*, $> 10^9$ s^{-1}, singlet excitons created on 4CzIPN-Me are immediately transferred to the S_1 state of TBRb, reducing the chance for ISC. Furthermore, this energy transfer is exothermic and a one-way process energetically, *i.e.*, the singlet excitons of TBRb cannot return to the S_1 state of 4CzIPN-Me.

Figure 3(a) and (b) show numerically calculated N_S and N_T on 4CzIPN-Me without FRET and with FRET for different k_{ET} by using Eqs. 2 and 3. By adding fluorescent molecules at a concentration of only 0.65mol%, corresponding to $k_{ET} = 10^9$ s^{-1}, the singlet density quickly decreases after excitation, leading to N_S that is four orders of magnitude lower ($\sim 10^{13}$ cm^{-3}) and N_T that is one order of magnitude lower ($\sim 10^{16}$ cm^{-3}) than those without FRET about 10 ns after a short pulse excitation of 1 ns. This indicates that the number of ISC/RISC cycles would be significantly reduced, leading to a decrease of triplet exciton population on 4CzIPN-Me.

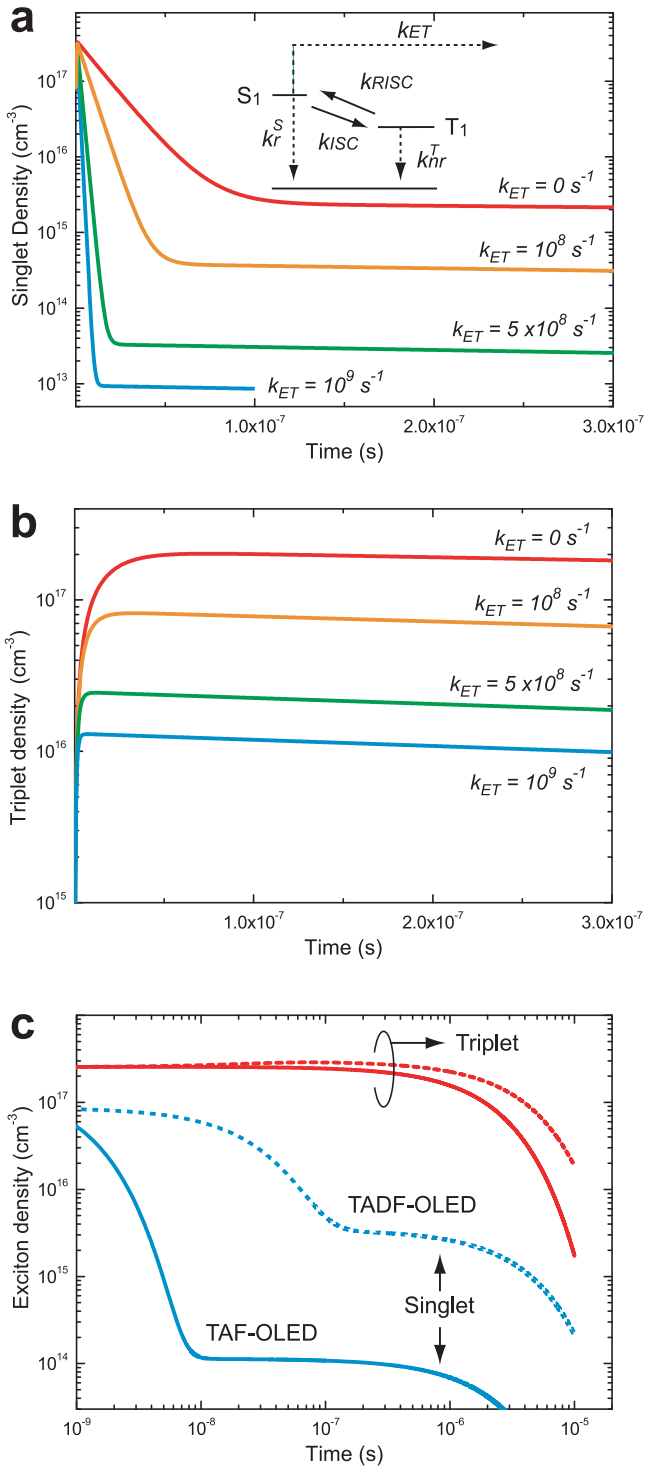

Figure 3 | Calculated singlet and triplet exciton densities. Dependence of calculated singlet density (a) and triplet density (b) in a 6.3mol%-4CzIPN-Me:mCBP co-deposited film on the rate constant of energy transfer (k_{ET}) as a function of time. The exciton density is calculated using Eqs. (2) and (3) with $k_{ISC} = 4.1 \times 10^7$ s^{-1}, $k_{RISC} = 7.7 \times 10^5$ s^{-1}and $k_r^S = 2.5 \times 10^7$ s^{-1} and $k_{nr}^T = 2.0 \times 10^5$ s^{-1}. (c) The calculated singlet (blue lines) and triplet (red lines) exciton densities in a 6.3mol%-4CzIPN-Me:mCBP co-deposited film under electrical excitation as a function of time with ($k_{ET} = 10^9$ s^{-1}, solid lines) or without ($k_{ET} = 0$ s^{-1}, dashed lines) Förster energy transfer using Eqs. (4) and (5).

In the case of electrical excitation, the equations (2) and (3) can be revised as

$$\frac{dN_S}{dt} = -k_{ET}N_S - k_r^S N_S - k_{ISC}N_S + k_{RISC}N_T + {}^{J}/_{4de}, \quad (4)$$

$$\frac{dN_T}{dt} = -k_{nr}^T N_T - k_{RISC}N_T + k_{ISC}N_S + {}^{3J}/_{4de}, \quad (5)$$

where J is the injected current density, d is the recombination zone thickness, and e is the electron charge. When the number of excitons generated by short electrical excitation (pulse width = 1 ns) is the same as that generated by the optical excitation (10^{26} cm^{-3}s^{-1}) at t = 0 s, *i.e.*, $P = J/de$, one order of magnitude higher N_T ($\sim 10^{17}$ cm^{-3}) than that of optical excitation is generated due to the higher branching ratio of triplet excitons, with the N_S and N_T dynamics plotted in Fig. 3(c). Comparing with TADF, a dramatic decrease of the singlet exciton density for TAF was also observed for electrical excitation within the first tens of nanoseconds, while an appreciable decrease of triplet excitons at a faster rate was identified on a μs-order time scale. In addition, the reduction of N_S (from $\sim 2.5 \times 10^{18}$ cm^{-3} to $\sim 8.2 \times 10^{16}$ cm^{-3}) and N_T (from $\sim 1.8 \times 10^{20}$ cm^{-3} to $\sim 8.0 \times 10^{19}$ cm^{-3}) was also confirmed for steady-state conditions, *i.e.*, $\frac{dN_S}{dt} = 0$ and $\frac{dN_T}{dt} = 0$. Thus, while the reduction of N_T by including FRET is weaker for electrical excitation than for optical excitation, the **TAF**-system clearly provides a way to reduce N_T in OLEDs.

Suppression of exciton annihilation process. A decrease in N_T and triplet exciton lifetime can have repercussions not only for operational stability but also for the exciton annihilation processes that lead to a decrease of η_{int} at high luminances. In our previous study, we clarified that the annihilation processes in **TADF-OLEDs** can be described by a combination of singlet-triplet annihilation (STA) and TTA[24]. How strongly each exciton annihilation process influences η_{int} as luminance increases in different **TADF-OLEDs** can be compared by considering the estimated critical current densities J_{TT} and J_{ST} where the initial luminance decays by half *via* TTA and STA, respectively, calculated by ref. 24

$$J_{TT} \sim \frac{ed\Phi_{prompt}k_{RISC}^2}{k_{TT}}, J_{ST} \sim \frac{ed\Phi_{prompt}k_r^S k_{RISC}}{k_{ST}}, \quad (6)$$

where k_{TT} and k_{ST} (in unit of cm^3 s^{-1}) are the rates of TTA and STA, respectively, and Φ_{prompt} is the prompt component of the PL efficiency. Considering these relationships, a **TAF**-system can be shown to suppress exciton annihilation in OLEDs.

We compared the roll-off characteristics in **TAF**- and **TADF-OLEDs** by using 4,5-di(9H-carbazol-9-yl)phthalonitrile (2CzPN) as the TADF molecule since 2CzPN-based OLEDs show rather strong roll-off characteristics as reported in our previous study[24]. To confirm that bimolecular interaction occurs in 2CzPN, we first measured the transient PL of 7.2mol%-2CzPN in an mCBP host matrix under pulse excitation with a rather long width of 500 μs, *i.e.*, quasi steady-state excitation, and an excitation power of $\sim$1.5 kW/cm^2. We also prepared a reference film of 6.3mol%-4CzIPN-Me doped into an mCBP host.

The PL characteristics and Jablonski diagrams of 2CzPN and 4CzIPN-Me are summarized in Table 2 and Fig. 4(a), respectively (see Supplementary note for details on the calculation of the rate

Table 2 | PL characteristics and rate constants of TADF molecules

TADF molecule	ΔE_{ST} [eV]	Total PL efficiency [%]	Φ_{prompt} [%]	$\Phi_{delayed}$ [%]	τ_p [ns]	τ_d [μs]	k_r^S [10^7 s^{-1}]	k_{nr}^T [10^5 s^{-1}]	k_{ISC} [10^7 s^{-1}]	k_{RISC} [10^5 s^{-1}]
4CzIPN-Me	0.05	74	38	36	15	2.0	2.5	2.0	4.1	7.7
2CzPN	0.29[a]	85	50	35	17	265	2.9	0.01	2.9	0.054

[a]The singlet and triplet energy levels of 2.95 eV and 2.66 eV were estimated from the onset of fluorescence and phosphorescence spectra, respectively.

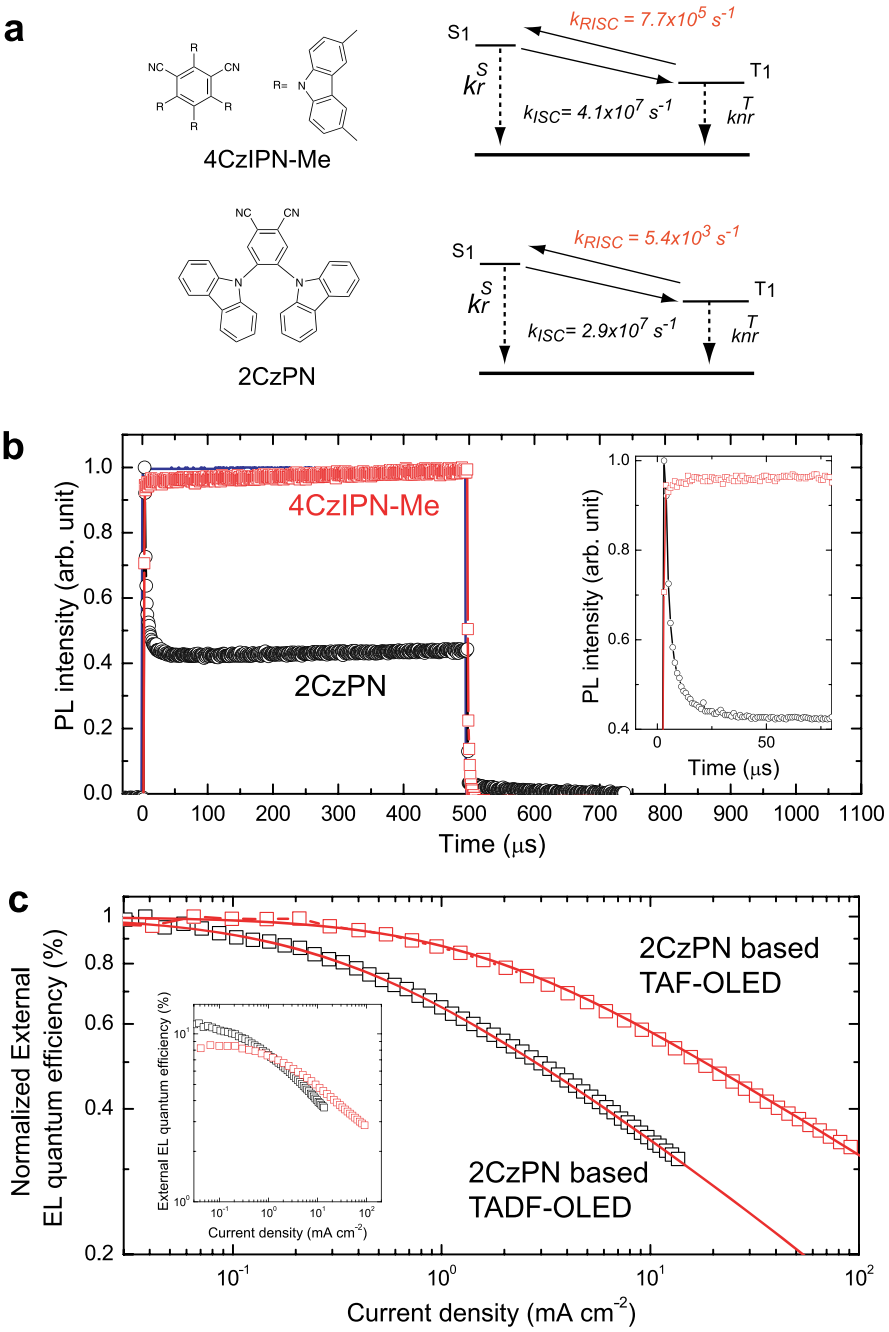

Figure 4 | Bimolecular annihilation characteristics. (a) The chemical structures and energetic process diagrams of 4CzIPN-Me and 2CzPN. (b) PL transient characteristics for 6.3mol%-4CzIPN-Me (red circles) or 7.2mol%-2CzPN (black circles) doped mCBP films. The films were pumped with a laser diode (excitation power of ~1.5 kW/cm^2) with pulse width of 500 μs at an excitation wavelength of 405 nm. The blue solid line indicates the time profile of the excitation beam. Inset: Close-up of PL transient signals immediately after excitation. For 2CzPN, the PL intensity rapidly decays to a steady-state intensity of 43% of the peak intensity within the initial 50 μs of excitation time. (c) Normalized external EL quantum efficiency as a function of injected current density for the 2CzPN-based OLEDs with (red squares) or without (black squares) 0.65mol%-TBRb. The OLED structure was ITO (100 nm)/HAT-CN (10 nm)/TAPC (30 nm)/7.2mol%-2CzPN:mCBP (30 nm)/T2T (10 nm)/Alq_3 (55 nm)/LiF (0.8 nm)/Al (100 nm). The solid lines correspond to the η_{EQE} calculated based on the exciton annihilation model. Inset: The actual external EL quantum efficiency as a function of injected current density for the tested OLEDs (coloured accordingly).

constants). While both co-deposited films show comparable Φ_{PL} and similar k_{ISC} and k_r^S of the order of $\sim 10^7$ s^{-1}, 2CzPN possesses a smaller k_{RISC} of $\sim 10^3$ s^{-1} due to its large ΔE_{ST} of $\sim$ 0.29 eV. This smaller k_{RISC} for 2CzPN is expected to lead to a larger triplet population since triplets will not be upconverted to singlets as quickly as for 4CzIPN-Me.

If the triplet population created by the balance between ISC from S_1 to T_1 and RISC from T_1 to S_1 is large enough to induce strong triplet-triplet absorption, the PL intensity will significantly decrease with increasing excitation time *via* STA as has been demonstrated for 4-(dicyanomethylene)-2-methyl-6-julolidyl-9-enyl-4H-pyran doped into tris(8-hydroxyquinoline)aluminum (Alq_3)[25]. In fact, we observed a clear dependence of the PL decay characteristics on the k_{RISC} values as shown in Fig. 4b. In the case of 2CzPN, a significant decrease of the PL intensity within the initial 50 μs of quasi steady-state optical excitation was clearly observed, indicating that a large population of triplet excitons on the T_1 state of 2CzPN due to the small k_{RISC} is inducing a reduction of the exciton density *via* bimolecular interaction during long pulse excitation.

This optical behavior is consistent with the rapid drop of η_{EQE} with an increase of injected current density in the OLED with 7.2mol%-2CzPN as an emissive dopant (Fig. 4(c)), resulting in a 50% decrease of η_{EQE} from the maximum at as low as 3 mA cm^{-2}. Fortunately, the **TAF** scheme provides a path for "one-way" triplet energy transfer from TADF molecules to end emitters, thus decreasing N_T on the TADF molecules and relaxing the bimolecular annihilation. In fact, when 0.65mol%-TBRb was added into a 7.2mol%-2CzPN:mCBP matrix as an exciton acceptor to form a **TAF-OLED**, the experimental current density at 50% luminance was calculated to be ~6-times higher (~18 mA cm^{-2}) than that of the corresponding **TADF-OLED**.

By fitting the model in Ref. 24 to the device characteristics in Fig. 4(c), the best agreement between experimental data and modeled curves were obtained with $k_{ST} = 5 \times 10^{-12}$ cm^3 s^{-1} and $k_{TT} = 2.5 \times 10^{-15}$ cm^3 s^{-1} for the **TADF-OLED** and $k_{ST} = 6 \times 10^{-13}$ cm^3 s^{-1} and $k_{TT} = 5 \times 10^{-16}$ cm^3 s^{-1} for the **TAF-OLED**. The reduction of k_{ST} and k_{TT} by one order of magnitude for the **TAF-OLED** compared to the **TADF-OLED** indicates that bimolecular annihilation can also be reduced by employing a **TAF**-system, which is attributed to rapid FRET decreasing the number of ISC/RISC cycles and, subsequently, the triplet population. In addition, we note that the observation of k_{ST} that is about three orders of magnitude larger than k_{TT} suggests that STA is the most dominant bimolecular annihilation process for excitons in OLEDs with TADF molecules.

Discussion

In summary, we demonstrated that both high electroluminescence efficiency and enhanced operational stability could be achieved in TAF-OLEDs by introducing an assistant dopant having a rather large k_{RISC}~10^6, 4CzIPN-Me. Furthermore, suppression of exciton annihilation was demonstrated *via* efficient and rapid triplet-singlet upconversion. We believe that development of TADF assistant dopants having even larger k_{RISC} will further improve OLED performance.

Methods

Materials. The materials 4,4′-cyclohexylidenebis[N,N-bis(4-methylphenyl) benzenamine] (TAPC) and 2,8-di[t-butyl]-5,11-di[4-(t-butyl)phenyl]-6,12-diphenyl naphthacene (TBRb) were purchased from Luminescence Technology Corp. Tris(8-hydroxyquinolinato)aluminum (Alq_3) was used as received from Nippon Steel Chemical Co., Ltd. Dipyrazino[2,3-f:20,30-h]quinoxaline-2,3,6,7,10,11-hexacarbonitrile (HAT-CN) and 3,3-di(9H-carbazol-9-yl)biphenyl (mCBP) were purchased from NARD Institute, Ltd. (2s,4r,6s)-2,4,5,6-tetrakis(3,6-dimethyl-9H-carbazol-9-yl)isophthalonitrile (4CzIPN- Me), 4,5-di(9H-carbazol-9-yl)phthalonitrile (2CzPN), and 2,4,6-tris(biphenyl-3-yl)-1,3,5-triazine (T2T) were synthesized according to reported procedures.

Sample preparation and optical characterization of organic thin films. Organic solid-state films with thicknesses of 100 nm were grown by thermal evaporation. Organic deposition was performed under vacuum at pressures of below 5×10^{-5} Pa. PL quantum efficiency was measured with an absolute PL quantum yield measurement system (C11347-01, Hamamatsu Photonics) under the flow of nitrogen gas with an excitation wavelength of 337 nm. Emission lifetimes and phosphorescence spectrum of 4CzIPN-Me were measured using a streak camera (C4334, Hamamatsu Photonics) and cryostat (Iwatani Industrial Gases Co.) with a nitrogen gas laser (KEN-X, Usho Optical Systems Co., Ltd.) as an excitation light source under a pressure of about 3 Pa.

Fabrication of OLEDs. Organic layers were formed by thermal evaporation. We prepared a **TAF-OLED** structure of ITO (100 nm)/HAT-CN (10 nm)/TAPC (30 nm)/0.65mol%-TBRb:6.3mol%-4CzIPN-Me:mCBP (30 nm)/T2T (10 nm)/Alq_3 (55 nm)/LiF (0.8 nm)/Al (100 nm). As references, OLEDs with an EML of either 0.65mol%-TBRb:mCBP (**FLU-OLED**) or 6.3mol%-4CzIPN-Me:mCBP (**TADF-OLED**), *i.e.*, 4CzIPN-Me as the emitter, were also examined. Effective device areas of 1 mm^2 were defined on the patterned-ITO substrates by a polyimide insulation layer using a conventional photolithography technique. After device fabrication, devices were immediately encapsulated with glass lids using epoxy glue in a nitrogen-filled glove box ($O_2 < 0.1$ ppm, $H_2O < 0.1$ ppm). Commercial calcium oxide desiccant (Dynic Co.) was included in each encapsulated package.

Characterization of OLEDs. The current density-voltage-luminance characteristics of the OLEDs were evaluated using a source meter (Keithley 2400, Keithley Instruments Inc.) and an absolute external quantum efficiency measurement system (C9920-12, Hamamatsu Photonics). Each EL spectrum was collected by an optical fiber connected to a spectrometer (PMA-12, Hamamatsu Photonics). The reproducibility of device performance of the presented devices was confirmed by measuring over four different samples. The operational lifetime was measured using a luminance meter (SR-3AR, TOPCON) at a constant DC current. All measurements were performed in ambient atmosphere at room temperature.

1. Baldo, M. A., O'Brien, D. F., Thompson, M. E. & Forrest, S. R. Excitonic singlet-triplet ratio in a semiconducting organic thin film. *Phys. Rev. B.* **60**, 14422-14428 (1999).
2. Baldo, M. A. *et al.* Highly efficient phosphorescent emission from organic electroluminescent devices. *Nature.* **395**, 151-154 (1998).
3. Baldo, M. A. *et al.* Very high-efficiency green organic light-emitting devices based on electrophosphorescence. *Appl. Phys. Lett.* **75**, 4-6 (1999).
4. Adachi, C., Baldo, M. A., Thompson, M. E. & Forrest, S. R. Nearly 100% internal phosphorescence efficiency in an organic light-emitting device. *J. Appl. Phys.* **90**, 5048-5050 (2001).
5. Watanabe, S., Ide, N. & Kido, J. High-Efficiency Green Phosphorescent Organic Light-Emitting Devices with Chemically Doped Layers. *Jpn. J. Appl. Phys.* **46**, 1186-1188 (2007).
6. Reineke, S. *et al.* White organic light-emitting diodes with fluorescent tube efficiency. *Nature.* **459**, 234-238 (2009).
7. Helfrich, W. & Schneider, W. G. Transients of Volume-Controlled Current and of Recombination Radiation in Anthracene. *J. Chem. Phys.* **44**, 2902-2909 (1966).
8. Pope, M. & Swenberg, C. E. *Electronic Processes in Organic Crystals* (Oxford University Press, New York, 1982), p. 64.
9. Yokoyama, D. *et al.* Dual efficiency enhancement by delayed fluorescence and dipole orientation in high-efficiency fluorescent organic light-emitting diodes. *Appl. Phys. Lett.* **99**, 123303-123305 (2011).
10. Pu, Y.-J. *et al.* Optimizing the Charge Balance of Fluorescent Organic Light-Emitting Devices to Achieve High External Quantum Efficiency Beyond the Conventional Upper Limit. *Adv. Mater.* **24**, 1765-1770 (2012).
11. Kondakov, D. Y., Pawlik, T. D., Hatwar, T. K. & Spindler, J. P. Triplet annihilation exceeding spin statistical limit in highly efficient fluorescent organic light-emitting diodes. *J. Appl. Phys.* **106**, 124510-124516 (2009).
12. Endo, A. *et al.* Thermally Activated Delayed Fluorescence from Sn^{4+}–Porphyrine Complexes and Their Application to Organic Light Emitting Diodes — A Novel Mechanism for Electroluminescence. *Adv. Mater.* **21**, 4802-4806 (2009).
13. Tanaka, H., Shizu, K., Miyazaki, H. & Adachi, C. Efficient green thermally activated delayed fluorescence (TADF) from a phenoxazine–triphenyltriazine (PXZ–TRZ) derivative. *Chem. Comm.* **48**, 11392-11394 (2012).
14. Uoyama, H. *et al.* Highly efficient organic light-emitting diodes from delayed fluorescence. *Nature* **492**, 234-238 (2012).
15. Nasu, K. *et al.* A highly luminescent spiro-anthraquinone-based organic light-emitting diode through thermally activated delayed fluorescence. *Chem. Commun.* **49**, 10385-10387 (2013).
16. Nakanotani, H. *et al.* Promising operational stability of high-efficiency organic light-emitting diodes based on thermally activated delayed fluorescence. *Sci. Rep.* **3**, 2127-2131 (2013).
17. Nakanotani, H. *et al.* High-efficiency organic light-emitting diodes with fluorescent emitters. *Nat. Commun.* **5**, 4016-4023 (2014).
18. Cho, Y. J., Yook, K. S. & Lee, J. Y. High Efficiency in a Solution-Processed Thermally Activated Delayed-Fluorescence Device Using a Delayed-Fluorescence Emitting Material with Improved Solubility. *Adv. Mater.* **26**, 6642-6646 (2014).

19. Förster, T. 10th Spiers Memorial Lecture. Transfer mechanisms of electronic excitation. *Discuss. Faraday Soc.* **27**, 7-17 (1959).
20. Schrögel, P. *et al.* Meta-linked CBP-derivatives as host materials for a blue iridium carbene complex. *Org. Electron.* **12**, 2047-2055 (2011).
21. Smith, L. H., Wasey, J. A. E. & Barnes, W. L. Light out coupling efficiency of top-emitting organic light-emitting diodes. *Appl. Phys. Lett.* **84**, 2986–2988 (2004).
22. Tanaka, D. *et al.* Ultra High Efficiency Green Organic Light-Emitting Devices. *Jpn.J. Appl. Phys.* **46**, L10–L12 (2007).
23. Burrows, P. E., Forrest, S. R., Zhou, T. X. & Michalski, L. Operating lifetime of phosphorescent organic light emitting devices. *Appl. Phys. Lett.* **76**, 2493-2495 (2000).
24. Masui, K., Nakanotani, H. & Adachi, C. Analysis of exciton annihilation in high-efficiency sky-blue organic light-emitting diodes with thermally activated delayed fluorescence. *Org. Electron.* **14**, 2721-2726 (2013).
25. Zhang, Y. & Forrest, S. R. Existence of continuous-wave threshold for organic semiconductor lasers. *Phys. Rev. B.* **84**, 241301-241304 (2011).

Acknowledgments

We would like to acknowledge Ms. Kei Morimoto for her sincere assistance with device preparation. This work was supported by Japan Science and Technology Agency (JST), ERATO, Adachi Molecular Exciton Engineering Project, and Grant-in-Aid for Young Scientists B; Grant Numbers 26810110.

Author contributions

H.N. developed the basic concepts. T.F. and H.N. conceived the idea for the manuscript and designed the experiments. The experiments were carried out by T.F. and H.N. M.I. constructed the STA measurement system. T.F., H.N., and C.A. wrote the manuscript. The project was supervised by C.A. All the authors discussed the results and contributed to the article.

Additional information

Supplementary information accompanies this paper at http://www.nature.com/scientificreports

Competing financial interests: The authors declare no competing financial interests.

How to cite this article: Furukawa, T., Nakanotani, H., Inoue, M. & Adachi, C. Dual enhancement of electroluminescence efficiency and operational stability by rapid upconversion of triplet excitons in OLEDs. *Sci. Rep.* **5**, 8429; DOI:10.1038/srep08429 (2015).